IEEE Access
Multidisciplinary | Rapid Review | Open Access Journal

Received 3 January 2024, accepted 26 January 2024, date of publication 5 February 2024, date of current version 21 February 2024.

Digital Object Identifier 10.1109/ACCESS.2024.3361947

RESEARCH ARTICLE

Mechanism and Modeling of Power Conversion Efficiency Degradation of Si Solar Cells Under Thermal Cycling

CHANGWOON HAN AND SEUNGIL PARK
Department of Mechanical Engineering, The State University of New York, Korea (SUNY Korea), Incheon 21985, Republic of Korea
Corresponding author: Changwoon Han (changwoon.han@sunykorea.ac.kr)

This work was supported in part by the National Research Foundation of Korea under Grant 2021R1F1A-1052595; and in part by the Korea Evaluation Institute of Industrial Technology, Republic of Korea, under Grant 20017488.

ABSTRACT This study investigates the degradation mechanism in the power conversion efficiency of Si solar cells under thermal cycling (TC) and explores mathematical models of the degradation curve. TC experiments were conducted for two sets of solar modules. A novel method was introduced and implemented to extract the parameters in the diode circuit model of solar cells using all experimental data points in the I-V curve. It was observed that both the series resistance and reverse saturation current increased after TC. When evaluating the increases using linear, exponential, and logarithmic functions, it was expected that the power output decreases to a range of 82 to 93 % after 5,000 TC if only the series resistance increases, while in the range of 86 to 94 % after 5,000 TC if only the reverse saturation current increases. The power drop mechanism of solar cells under TC can be attributed to the cracking of the solder layer due to TC, which increases not only the series resistance but also the reverse saturation current, resulting in drops in the power output of the solar cell. A goodness-of-fit analysis reveals that a stretched exponential model best represents the power drop function of a solar cell under TC.

INDEX TERMS Si solar cell, thermal cycling, power degradation mechanism, power degradation curve.

I. INTRODUCTION

Solar cell modules installed outdoors lose their power conversion efficiency over time. The amount of power loss during a certain period is an important parameter of the solar cell module. Therefore, many efforts have been made to analyze, evaluate, and improve the parameters since solar cell modules were on the market. The thermal cycling (TC) environment, which is caused naturally by the temperature difference between day and night or the summer and winter seasons, is known to be a detrimental stress among all thermal environments that degrade the power conversion efficiency of solar cells [1]. Owing to this effect, solar cell modules must pass a certain amount of TC in an accelerated test mode to be certified by standards [2].

The associate editor coordinating the review of this manuscript and approving it for publication was Shuo Sun.

The mechanism of power drop under TC has been investigated by many researchers. Skoczek et al. [3] reported that TC in the IEC 61215 test sequence causes thermomechanical fatigue to the interconnections and leads to an increase in the series resistance of the solar cell module. Through analyses and experiments, Jeong et al. [4], [5] proved that TC causes the solder joints to crack in ribbon wires, thereby increasing the series resistance. Sharma and Chandel [6] found that structural changes in the solder layer due to thermomechanical fatigue result in increased series resistance and reduced performance. In a more recent study, Kumar and Gupta [7] supported the idea that the power loss associated with TC is mainly due to the increase in series resistance. Through simulations, Asadpour et al. [8] showed that solder bond failure manifests a distinct signature of series resistance in the fill factor (*FF*) and slope of the current-voltage (I-V) curve. The consensus of these studies is that TC causes the cracking

of the solder layer, and the cracks lead to an increase in series resistance, which causes the power output of the solar cell to drop.

Another issue related to the power drop is the mathematical model of degradation curve. Approximating and assuming the degradation curves to exhibit linearity would have been an obvious preliminary choice, but different degradation curves have been observed during the performance in the field [9]. The correct choice of degradation curve is important as it affects the prediction of the solar cell lifetime and the calculation of the levelized cost of energy. However, the degradation curve under TC has not been extensively discussed so far.

This study investigates the degradation mechanism of power conversion efficiency under TC through extensive experiments and analysis. First, TC tests were conducted for one-cell modules while periodically measuring the I-V curve. Second, a new method of estimating the parameters in the diode equivalent circuit model of a solar cell from the measured I-V curves under degradation was suggested and implemented for the experimental data. Third, it was shown that not only the series resistance but also the reverse saturation current increased significantly during TC. Next, based on this analysis, the degradation of the series resistance and reverse saturation current were modeled. The degradation models predicted the long-term behavior of power conversion efficiency under TC. Finally, the effects of the series resistance and reverse saturation current on the power drop under TC were compared. In addition, a goodness-of-fit test was conducted, and a mathematical function for the power drop under TC was suggested. This study shows that TC increases not only the series resistance but also the reverse saturation current of the solar cell, the effects of both parameters on the power drop are quantitatively comparable, and the degradation of power conversion efficiency due to TC can be modeled by a stretched exponential function.

II. EXPERIMENTS

To explore the degradation of the power conversion efficiency of solar cells due to TC, two sets of Si one-cell module samples, namely set A and B, were prepared. Figure 1 illustrates these sets of modules. The solar modules consisted of glass, a layer of ethylene vinyl acetate (EVA), a Si wafer, another layer of EVA, and a back sheet from top to bottom, and their properties are summarized in Table 1.

TC experiments of 1,000 cycles were conducted for sets A and B under the IEC 61215 [2] standard, which involves cycling the temperature between −40 and 85 °C for 4 h with 30 min of dwell time. TC chambers manufactured by ESPEC (model: TSA-41LA) were used in the experiment. Three and five samples were tested for sets A and B, respectively. Before the experiments and after every 200 TCs, the I-V curves of the modules were measured with K3000 (McScience) under the Standard Test Condition [2]. Note that measurements at 600 and 800 TCs were absent in set A owing to resource limitations. It is also noteworthy that the effect of TC on a solar module varies from the impact of solar irradiance on the operation of a PV module outdoors in environmental conditions. In an outdoor PV module, the temperature rise in the silicon layer results not only from heat conduction from the glass and back sheet layers but also from the internal absorption and thermalization of electrons and holes.

TABLE 1. Properties of experiment sample sets.

Module set	One-cell module A (Set A)	One-cell module B (Set B)
Number of cells in module	1	1
Si wafer	Mono-crystalline 0.17 mm	Mono-crystalline 0.17 mm
Active cell area	156x156 mm^2	156x156 mm^2
Glass thickness	3.2 mm	3.2 mm
Back sheet	PET-based 3 layers total 0.29 mm	PET-based 3 layers total 0.29 mm
Number of ribbon wires in a cell	5	4
Ribbon wire width	1.6 mm	1.6 mm
Solder type	Sn60Pb40	Sn60Pb40
EVA thickness (top and bottom)	0.25 mm	0.25 mm
Number of samples	3	5

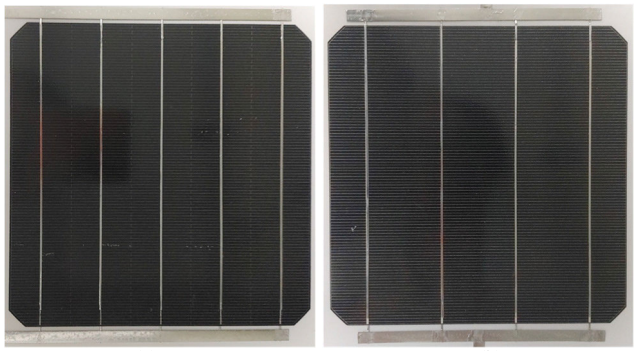

(a) (b)

FIGURE 1. Experiment samples: ones of (a) set A and (b) set B.

Parts of the experimental results are shown in Figs. 2 and 3 for sets A and B, respectively. They depict the degradation pattern of the open-circuit voltage (V_{oc}), short-circuit current (I_{sc}), FF, and maximum power (P_m) of the I-V curves during TC at normalized scales. The P_m dropped to between 92–96 % in the experiments after 1,000 TCs. The decrease in P_m was dominantly reflected by a decrease in the FF, but the V_{oc} also showed significant reduction. The FF was between 95– 98 %, while the V_{oc} was between 97–99 % after 1,000 TCs. The I_{sc} did not drop during TC, even though there were some fluctuations due to experimental uncertainty. As the FF is directly related to the series resistance of solar cells,

a decrease in FF is expected, but the decrease in V_{oc} cannot be explained by the change in series resistance.

III. PARAMETERS ESTIMATION OF EQUIVALENT CIRCUIT MODEL

A. PARAMETERS ESTIMATION METHOD

The one-diode equivalent circuit model of a solar cell is given in implicit form for I and V as

$$I = I_{ph} - I_o\left[exp\left(\frac{V+R_sI}{aV_T}\right)-1\right]-\frac{V+R_sI}{R_{sh}}, \quad (1)$$

where $V_T = N_skT/q$. When the temperature (T) and diode ideality factor (a) are known, the equation has four parameters: I_{ph}, I_o, R_s, and R_{sh}, which are the photocurrent, reverse saturation current, series resistance, and shunt resistance, respectively. Obtaining these parameters requires a set of test data, and many methods to obtain these parameters have been studied previously [10]. Most of them use specific points of the I-V curve, such as V_{oc}, I_{sc}, V_m (voltage at P_m), and I_m(current at P_m), because most manufacturers provide only these parameters [10]. However, the method based on selected points in the I-V curve does not fit the I-V curve well when the solar cell degrades [11].

Instead of using some specific points, all available data points of the I-V curve can be used to extract the parameters. First, inserting the three points of the I-V curve, (I_{sc}, 0), (0, V_{oc}), and (I_m, V_m) into Eq. (1) yields the following equations:

$$I_{sc} = I_{ph} - I_o\left[exp\left(\frac{R_sI_{sc}}{aV_T}\right)-1\right]-\frac{R_sI_{sc}}{R_{sh}} \quad (2)$$

$$0 = I_{ph} - I_o\left[exp\left(\frac{V_{oc}}{aV_T}\right)-1\right]-\frac{V_{oc}}{R_{sh}}, \quad (3)$$

$$I_m = I_{ph} - I_o\left[exp\left(\frac{V_m+R_sI_m}{aV_T}\right)-1\right]-\frac{V_m+R_sI_m}{R_{sh}} \quad (4)$$

Eqs. (2) to (4) result in

$$I_{sc} = I_o\left[exp\left(\frac{V_{oc}}{aV_T}\right)-exp\left(\frac{R_sI_{sc}}{aV_T}\right)\right]+\frac{V_{oc}-R_sI_{sc}}{R_{sh}}, \quad (5)$$

$$I_m = I_o\left[exp\left(\frac{V_{oc}}{aV_T}\right)-exp\left(\frac{V_m+R_sI_m}{aV_T}\right)\right] + \frac{V_{oc}-V_m-R_sI_m}{R_{sh}} \quad (6)$$

Eq. (5) yields R_{sh} as a function of R_s and I_o as follows:

$$R_{sh} = \frac{V_{oc}-R_sI_{sc}}{I_{sc}-I_o\left[exp\left(\frac{V_{oc}}{aV_T}\right)-exp\left(\frac{R_sI_{sc}}{aV_T}\right)\right]} \quad (7)$$

Next, Eqs. (3) and (7) lead to the relation of I_{ph} as a function of R_s and I_o as follows:

$$I_{ph} = I_o\left[exp\left(\frac{V_{oc}}{aV_T}\right)-1\right]+\frac{V_{oc}}{V_{oc}-R_sI_{sc}}\left[I_{sc}-I_o\left[exp\left(\frac{V_{oc}}{aV_T}\right)-exp\left(\frac{R_sI_{sc}}{aV_T}\right)\right]\right] \quad (8)$$

Inserting Eqs. (7) and (8) into Eq. (1) transforms Eq. (1) into a nonlinear equation with two independent variables, R_s and I_o as follows:

$$I = I_o\left[exp\left(\frac{V_{oc}}{aV_T}\right)-exp\left(\frac{V+R_sI}{aV_T}\right)\right] - \frac{V-V_{oc}+R_sI}{V_{oc}-R_sI_{sc}} \left\{I_{sc}-I_o\left[exp\left(\frac{V_{oc}}{aV_T}\right)-exp\left(\frac{R_sI_{sc}}{aV_T}\right)\right]\right\} \quad (9)$$

Finally, with Eqs. (5) and (6), we obtain I_o as a function of one variable R_s as follows: Inserting Eq. (10), as shown at the bottom of the page, into Eq. (9) transforms Eq. (1) into a nonlinear equation with one independent variable R_s as follows:

$$I = f(V) \quad \text{with variable } R_s \text{ and constants } V_{oc}, I_{sc}, V_m, \text{ and } I_m. \quad (11)$$

R_s can be extracted using the nonlinear least squares method on Eq. (11). Subsequently, I_o can be obtained using Eq. (10). The algorithm for parameter extraction from the diode equivalent circuit model with I-V data is shown in Fig. 4.

B. ESTIMATION OF THE DIODE IDEALITY FACTORS

The ideality factor is a parameter that describes how closely the I-V characteristics of a device match the theoretical behavior predicted by the ideal diode equation. In the case of recombination in the space-charge region, the ideality factor is typically between 1 and 2 [12]. It has been reported that all major aspects of non-ideal characteristics are due to extended cell crystal defect [13].

The ideality factors, a, in Eq. (1) can be estimated by utilizing the suggested process shown in Fig. 4. By changing a between 1 and 2, the residual between the experimental data and Eq. (1) was calculated, and the minimum value determined a. The calculated a during the thermal cycling was shown in Fig. 5 for sets A and B. No significant trend of either increasing or decreasing was observed, indicating that severe defects were not developed in the Si cell during TC. The averaged values of a are 1.15 and 1.28 for sets A and B, respectively.

C. PARAMETERS ESTIMATION RESULTS

With the assessed a values at Sec. B, the suggested method at Sec. A was implemented for all I-V data of sets A and B. The I-V curves for a sample (B-4) during TC are shown as an example in Fig. 6, and the modeling results of the

$$I_o = \frac{V_{oc}(I_{sc}-I_m)-I_{sc}V_m}{exp\left(\frac{V_m+R_sI_m}{aV_T}\right)(V_{oc}-R_sI_{sc})-exp\left(\frac{V_{oc}}{aV_T}\right)(V_m+R_s(I_m-I_{sc}))-exp\left(\frac{R_sI_{sc}}{aV_T}\right)(V_{oc}-V_m-R_sI_m)} \quad (10)$$

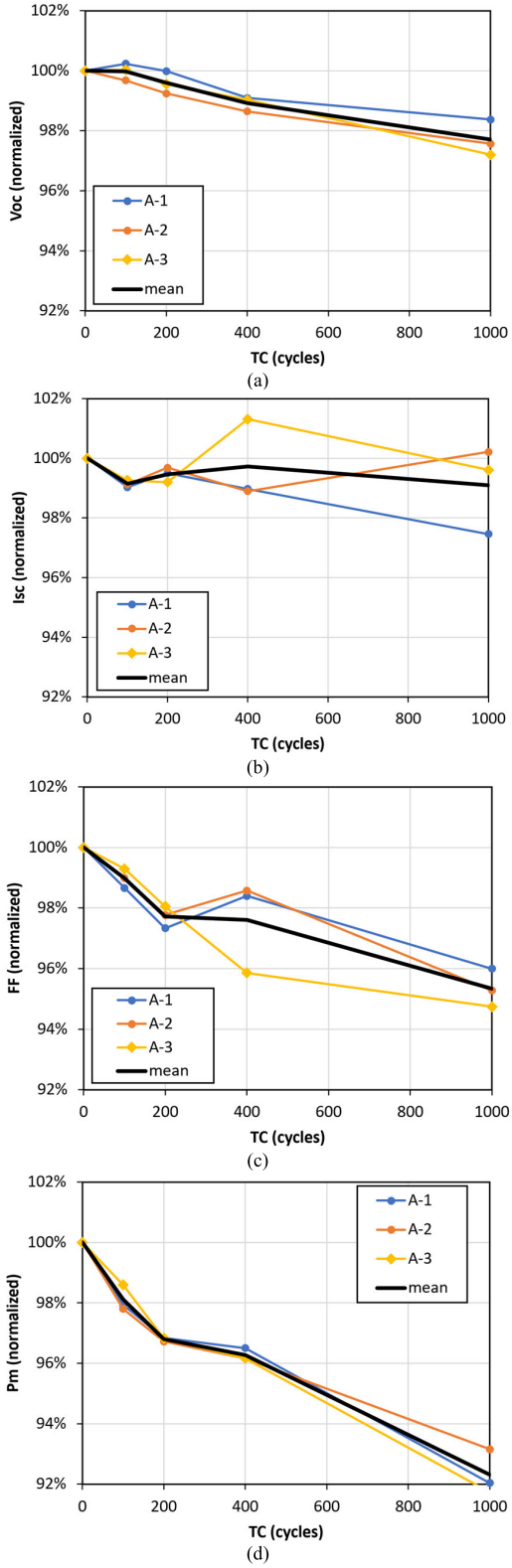

FIGURE 2. Experimental results of set A: (a) V_{oc}, (b) I_{sc}, (c) FF, and (d) P_m drop over TC.

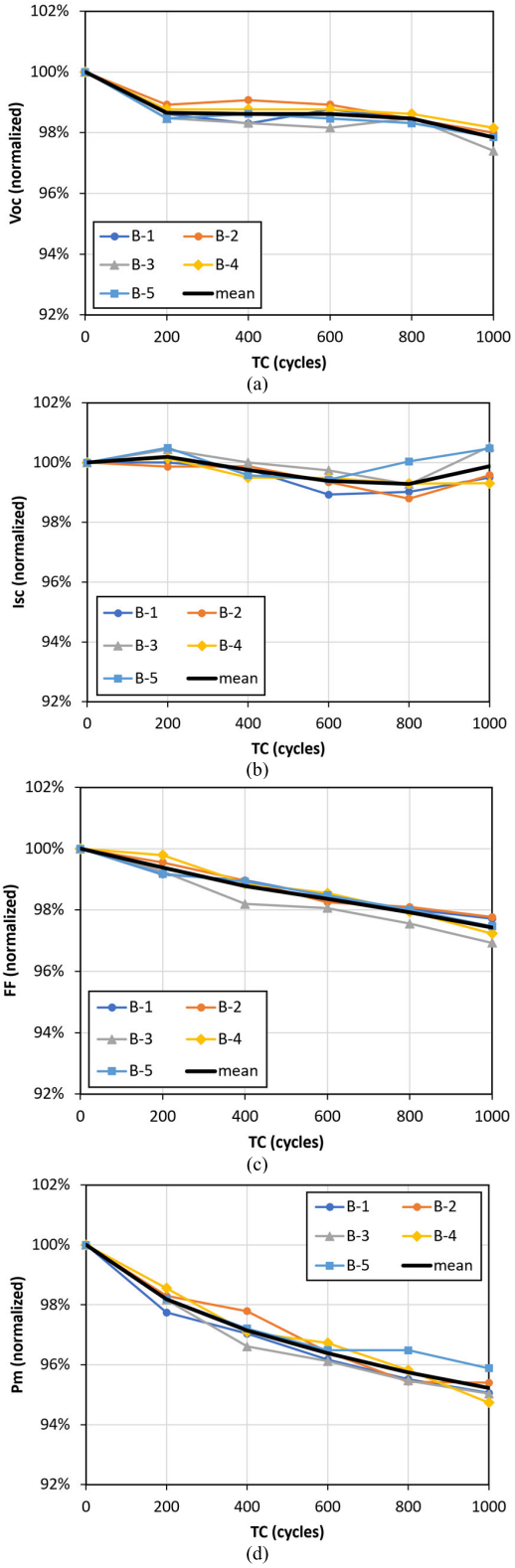

FIGURE 3. Experimental results of set B: (a) V_{oc}, (b) I_{sc}, (c) FF, and (d) P_m drop over TC.

I-V curves are represented in Fig. 7. The estimations by the extracted parameters of the diode model match well with the experiment for all degraded data, which demonstrates the validity of the proposed method.

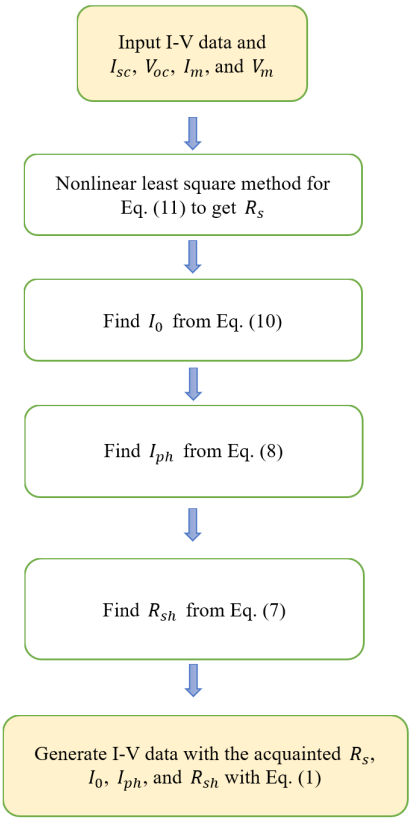

FIGURE 4. Algorithm of parameters extraction from the diode equivalent circuit model.

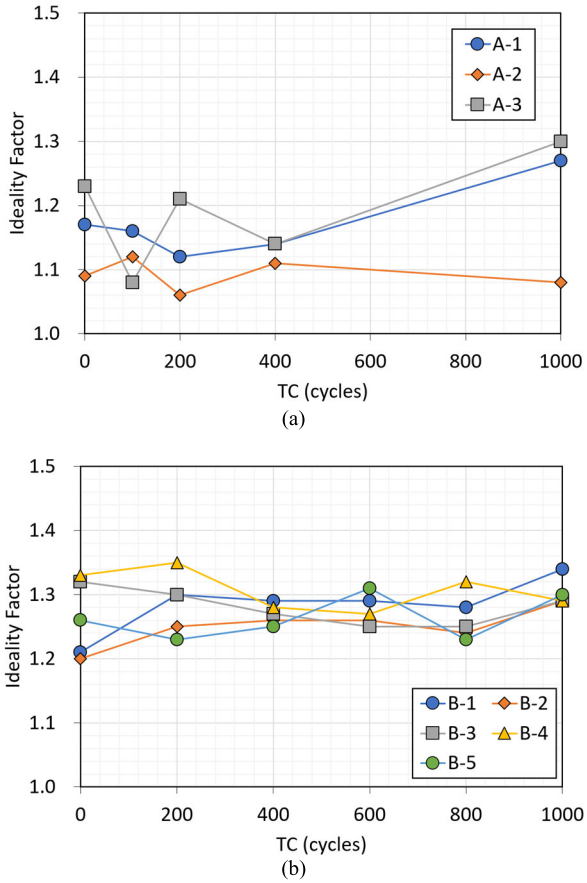

FIGURE 5. Calculated ideality factors over TC for (a) sets A and (b) B.

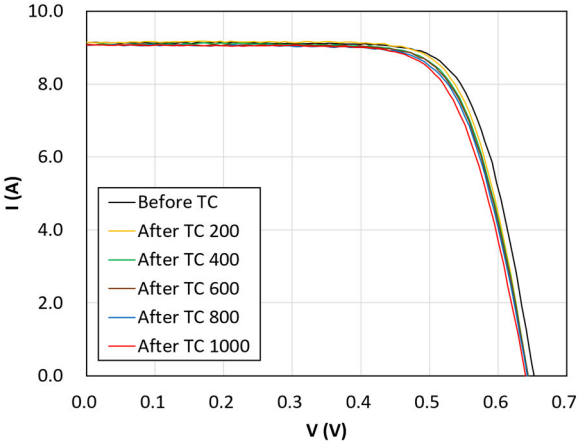

FIGURE 6. I-V curves during TC for sample B-4.

Using the method, the extracted parameters, R_s and I_o, for all sample sets are shown in Fig. 8. The observations revealed that both I_o and R_s increased during TC. Over 1,000 TCs, R_s and I_o increased between 13–42 % and 38–83 %, respectively. The parameters I_{ph} and R_{sh} did not change with TC.

D. INTERPRETATION OF R_S AND I_O INCREASES

A previous study by the author simulated the cracking in the solder layer of a Si solar cell under TC, as well as the resulting changes in electric potential and increase in R_s, using FEM [14]. When a crack appears in the solder layer, it alters the potential contour in its vicinity, as shown in Fig. 9(a) for the cases of intact and cracked solder layers, and causes the current to flow around it, as demonstrated in Fig. 9(b). This results in a decrease in the net current flow at the busbar and the increase in R_s. The details of FE modelling for Fig. 9 can be found in reference [14] and are not repeated here.

The change of electric field in the cell from the cracks also impacts the minority carrier diffusion length in the area. It was demonstrated experimentally. Electroluminescence (EL) technique captures light emission from solar cells under forward bias by a CCD camera. Its intensity distribution of emission is proportional to the minority carrier diffusion length in Si solar cells [15]. Figure 10 shows EL technique images of the cells A-3 and B-1 before and after TC 1000 cycles. EL images of the cell were measured by K3200 ELX (McScience). In the images after TC 1000 cycles of Fig. 10, long, dark, and rectangles dangled from the ribbon wires can be found. They were referred to as rectangular dark areas (RDAs) and it was shown that the locations of the RDA coincided with the locations of the cracks in the solder layer and the RDA incidence in cells increased proportionally over TC [16]. The I_o represents the thermal recombination current

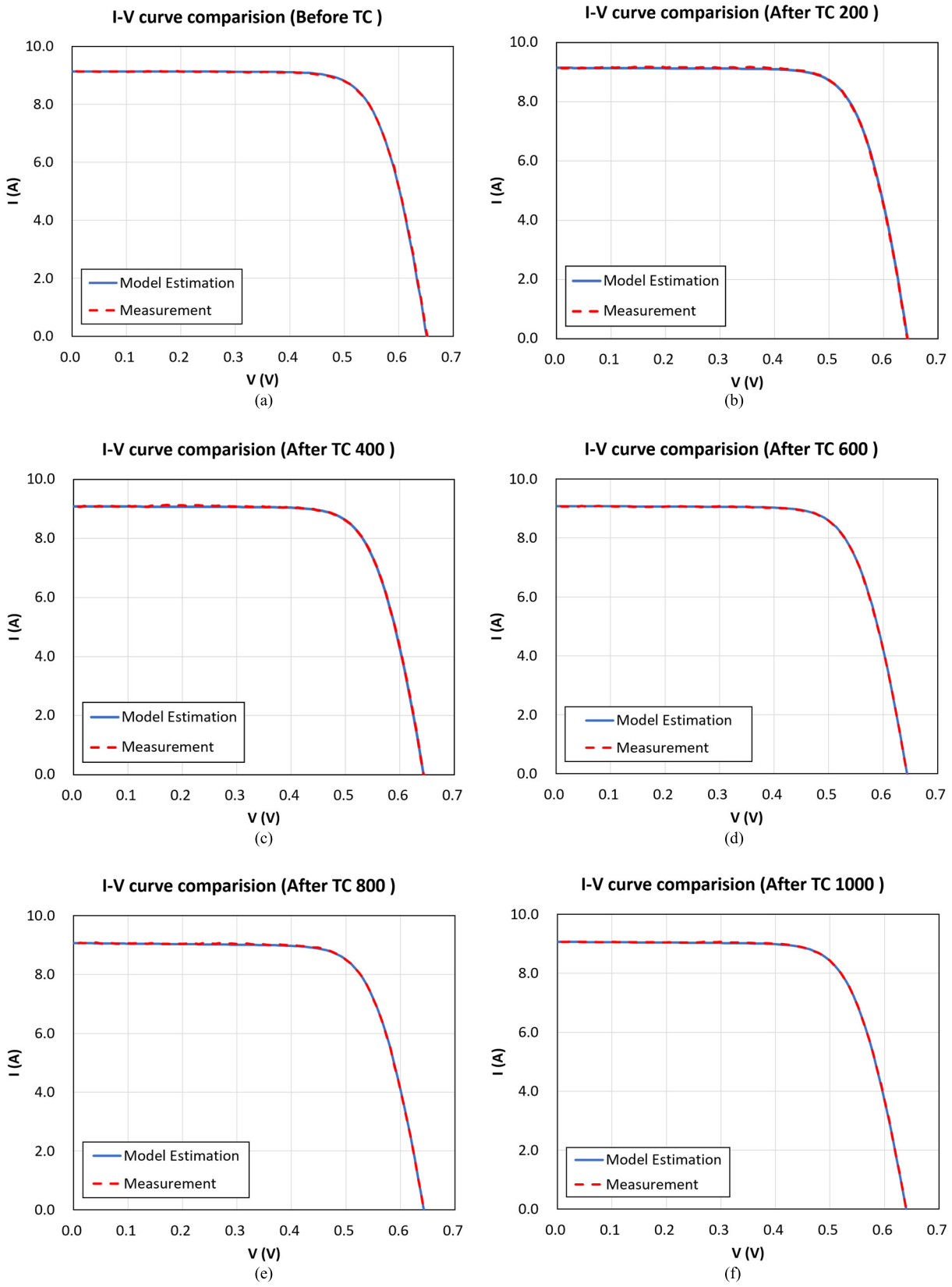

FIGURE 7. Comparison of the I-V curves (measured vs. modeled from the estimations) for sample B-4 at following values of TC: (a) 0, (b) 200, (c) 400, (d) 600, (e) 800, and (f) 1,000.

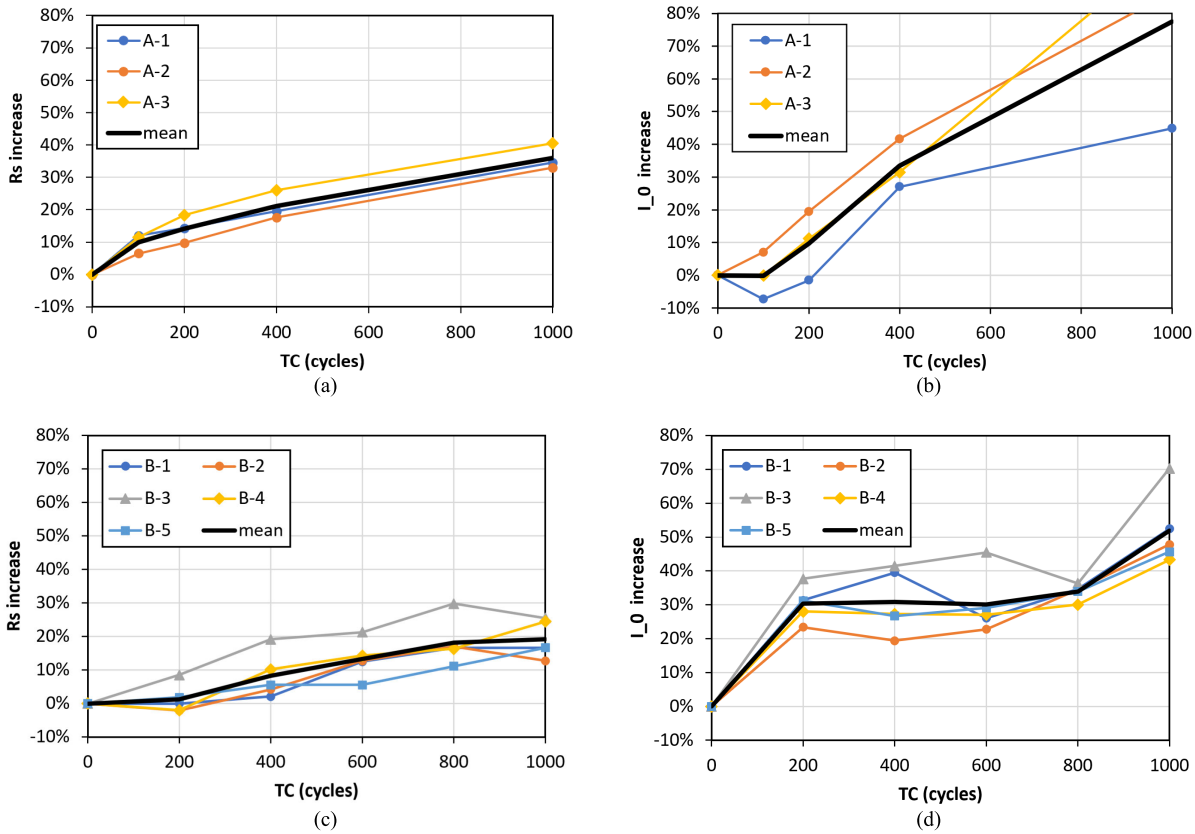

FIGURE 8. Results of extracted parameters, R_S and I_O, over TC for: (a, b) set A and (c, d) set B.

in solar cells [17]. If the minority carrier diffusion length decreased locally by the cracks as indicated by the EL images, this would lead to an increase in recombination current and ultimately result in an increase in I_o.

IV. Effect of R_S AND I_o INCREASE ON LONG-TERM POWER DROP

A. MODELING OF R_S AND I_o INCREASE

The effect of R_s and I_o increase on the long-term power drop was evaluated. First, R_s and I_o are modeled functionally. However, functional models for R_s and I_o during the degradation in long term under TC have not been investigated extensively, and experimental data is lacking. A simulation study showed that R_s is increasing exponentially during TC over the crack ratio at the solder layer [14] as shown in Fig. 11. But the analysis didn't provide a relation between TC and the crack ratio.

In this study, to account for the uncertainty in the functional models, we modeled R_s and I_o with different functional forms. Specifically, linear, exponential, and logarithmic increases are adapted for extrapolation and wide-ranging evaluation, as follows:

Linear model:

$$\frac{R_s(N)}{R_s(0)} \; and \; \frac{I_0(N)}{I_0(0)} = AN + 1, \tag{12a}$$

Exponential model:

$$\frac{R_s(N)}{R_s(0)} \; and \; \frac{I_0(N)}{I_0(0)} = exp(AN), \tag{12b}$$

Logarithmic model:

$$\frac{R_s(N)}{R_s(0)} \; and \; \frac{I_0(N)}{I_0(0)} = ln(AN + 1) + 1, \tag{12c}$$

where N is the number of TCs, and A is the model constants. Linear regression results for the Eq. (12) with the data of Fig. 8 are summarized in Table 2.

TABLE 2. Linear regression results for A values in Eq. 12.

Model	Regression model constants (A, unit: 1/TC)	
	for R_s	for R_s
Linear	2.68×10^{-4}	5.56×10^{-4}
Exponential	2.40×10^{-4}	4.56×10^{-4}
Logarithmic	3.04×10^{-4}	7.19×10^{-4}

To investigate the effects of R_s and I_o on long-term or up to 80 % power loss, which is the typical warranty limit for solar cell manufacturers [18], R_s and I_o values were calculated over 5,000 TCs with three regression models, as shown in Fig. 12. After 5,000 TCs, R_s are expected to increase 92 %, 134 %,

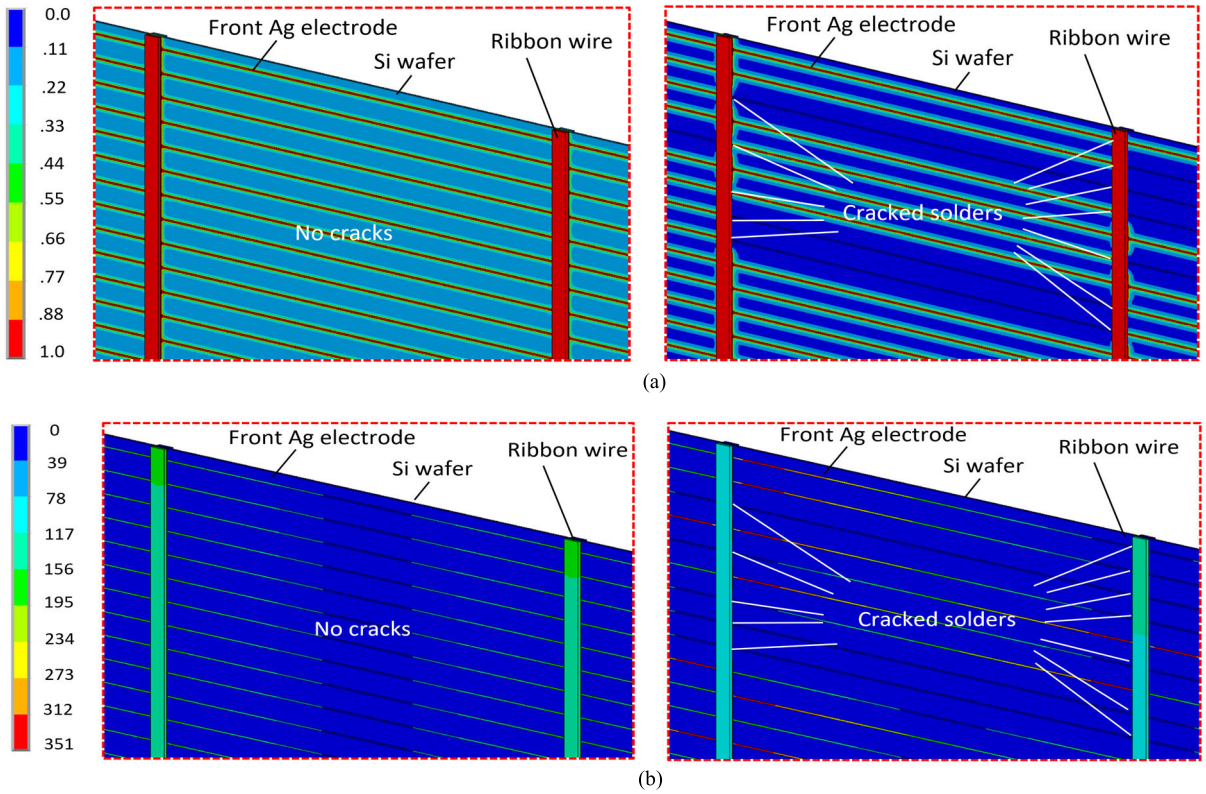

FIGURE 9. FE simulation results presented for the cases of intact solder layers (left) and cracked solder layers (right), with contour plots depicting the (a) electric potential and (b) current density.

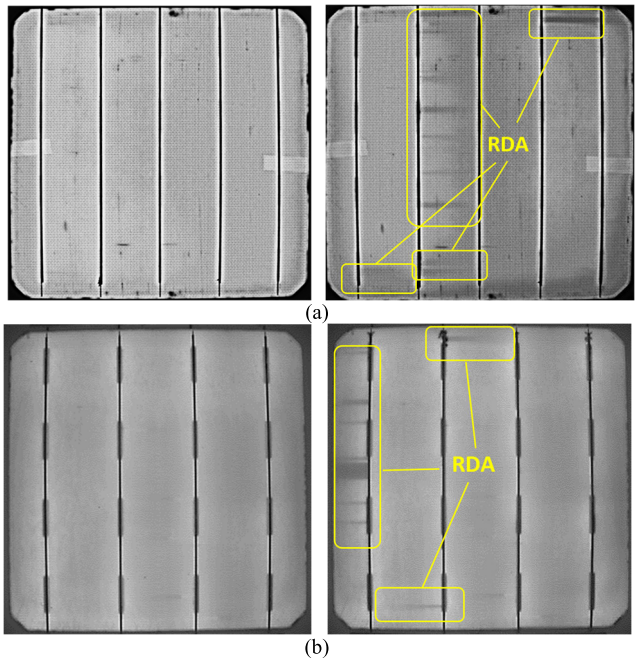

FIGURE 10. EL images of samples (a) A-3 and (b) B-1 before (left) and after TC 1,000 cycles (right).

and 231 % for the logarithmic, linear, and exponential model, respectively, while I_o are expected to increase 153 %, 278 %, and 878 % for the logarithmic, linear, and exponential model, respectively.

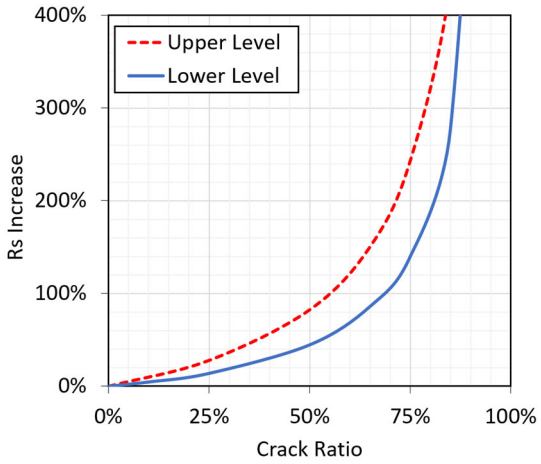

FIGURE 11. FE simulation results for R_S increase over crack ratio.

B. COMPARISON OF EFFECT OF R_S AND I_O INCREASE ON POWER DROP

Based on the data of the sample sets A and B, a one-diode equivalent circuit model for a one-cell module with $R_s = 0.005\ \Omega$, $I_o = 1.5\text{e-}8$ A, $R_{sh} = 25\ \Omega$, $I_{ph} = 9$ A, $a = 1.25$, and $T = 298$ K was constructed using the SPICE simulation

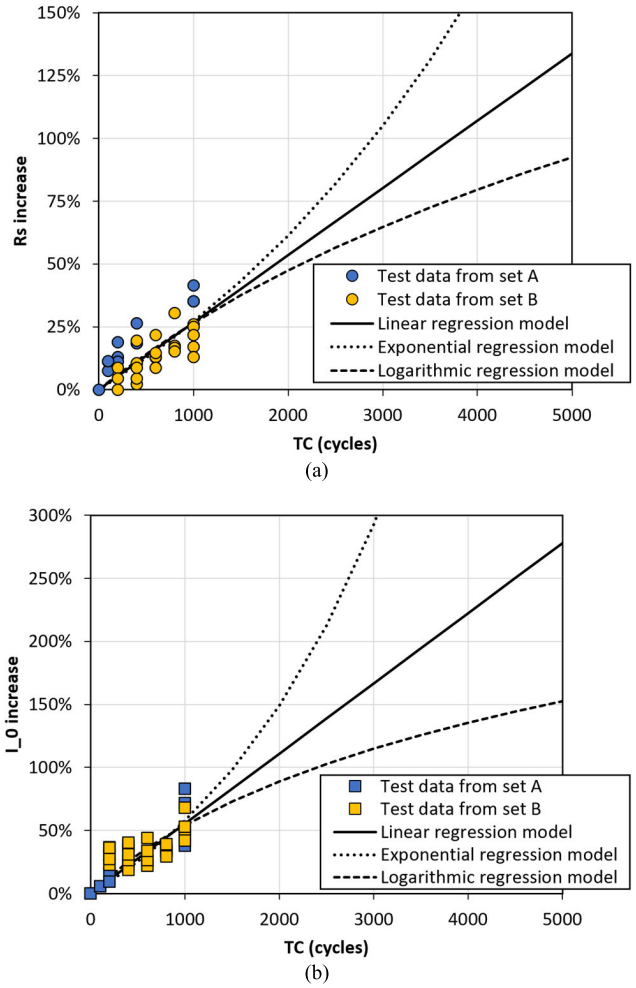

FIGURE 12. Prediction of (a) R_s and (b) I_o increase over 5,000 TCs with three different functional models.

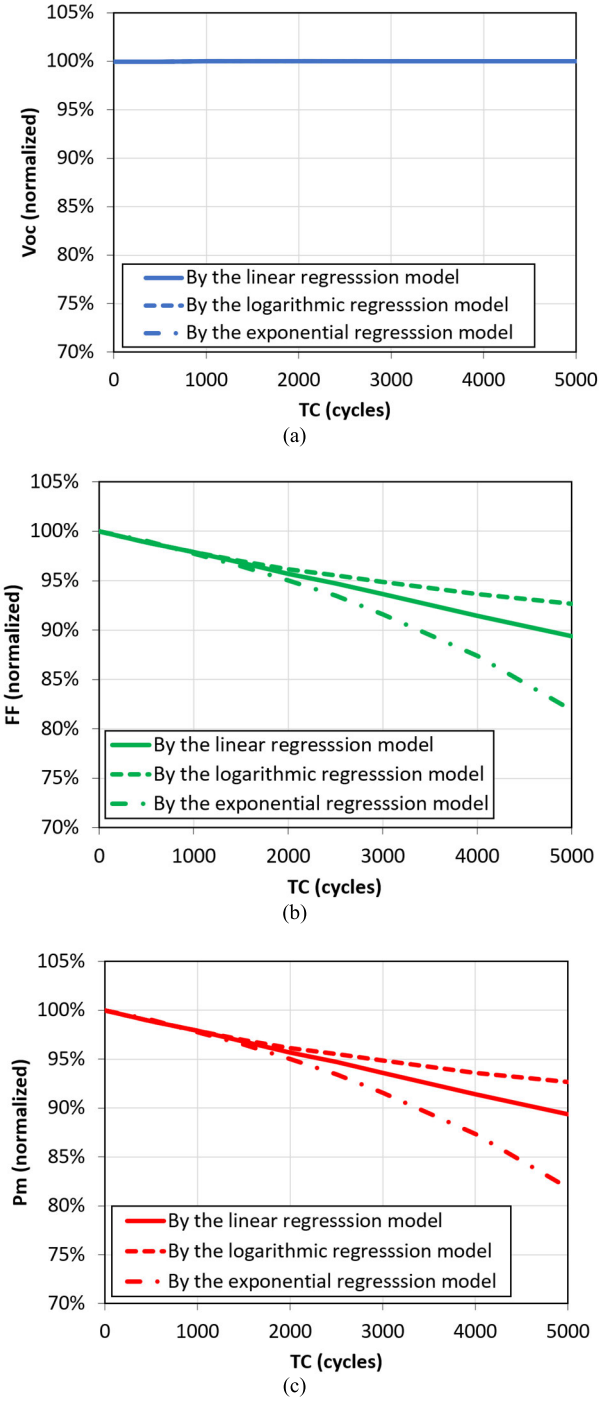

FIGURE 13. Plots of simulated (a) V_{oc}, (b) FF, and (c) P_m drop over TC when assuming R_s only increases with TC.

software application [19]. The model with the expected R_s and I_o values from Fig. 12 was used to calculate the I-V curves and their corresponding parameters under different TC conditions. The results are presented in Figs. 13 to 15. Figures 13 and 14 show the prediction results of V_{oc}, FF, and P_m over TC based on the three regression models of R_s and I_o for the assumption of R_s only (Fig. 13) and I_o only (Fig. 14). Figure 15 compares P_m drops caused by R_s and I_o increases, as well as their combination, for the linear, logarithmic, and exponential assumptions.

If only R_s increases with TC and I_o remains unchanged, it is expected that V_{oc} does not change, but FF drops with constant, increasing, and decreasing rate for the model of linear, logarithmic, and exponential, respectively, as shown in Fig. 13. It was expected that power drops to in the range of 92 to 95 % at 3,000 TC, or in the range of 82 to 93 % after 5,000 TC. On the other hand, if only I_o increases with TC, it is expected that V_{oc} and FF drop with constant rate for the exponential model but with decreasing rates for the model of linear and logarithmic; consequently, the power drops in the same manner as shown in Fig. 14. It was expected that power drops to in the range of 92 to 95 % at 3,000 TC, or in the range of 86 to 94 % after 5,000 TC.

The ratio of power drop with an increase in R_s and I_o is approximately equal, indicating the effect of each parameter on the power drop is comparable. The effect of increased I_o on the power drop reduces with increased

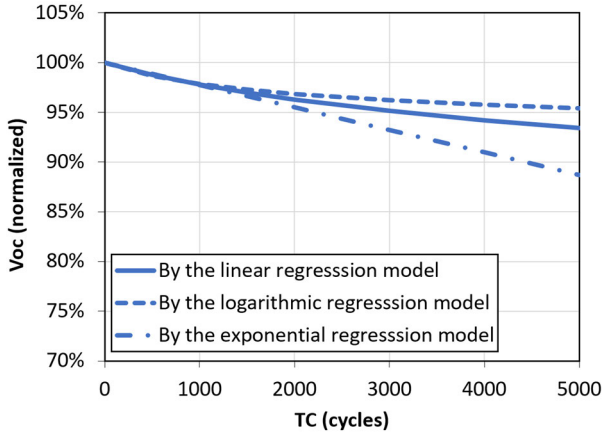

(a)

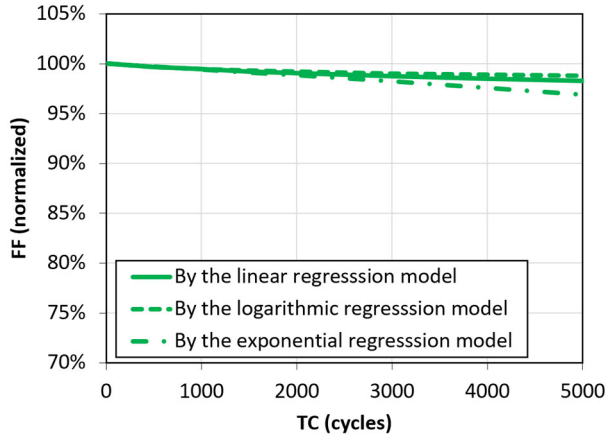

(b)

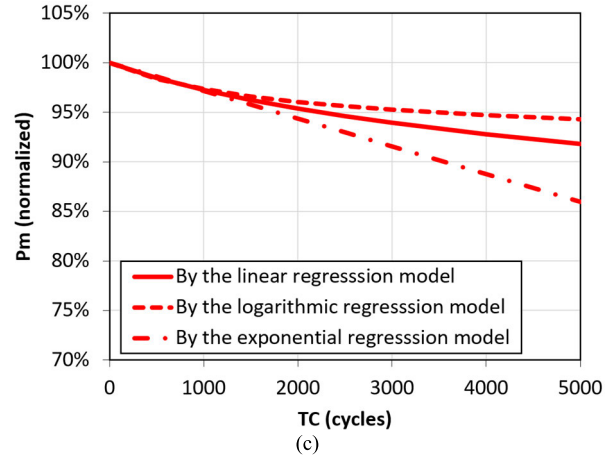

(c)

FIGURE 14. Plots of simulated (a) V_{oc}, (b) FF, and (c) P_m drop over TC when assuming I_o only increases with TC.

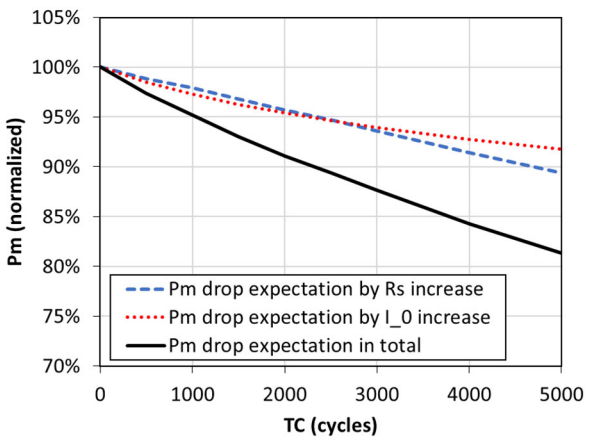

(a)

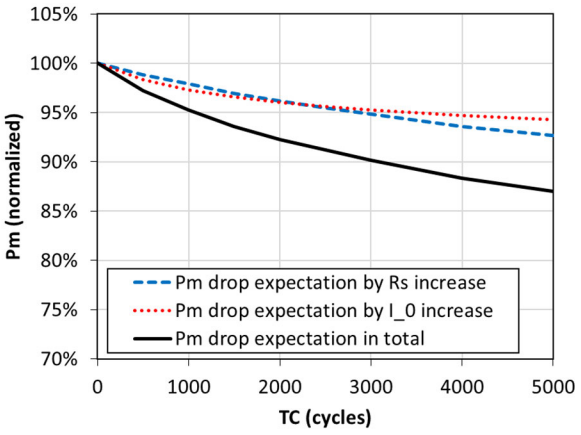

(b)

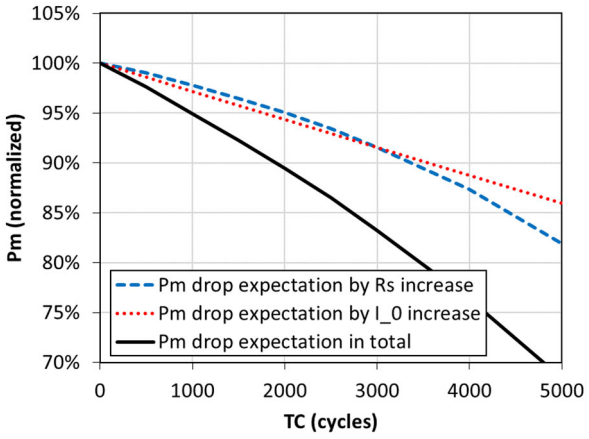

(c)

FIGURE 15. Comparisons of P_m drops caused by R_s and I_o increase, as well as their combination, for the (a) linear, (b) logarithmic, and (c) exponential assumptions of R_s and I_o.

TCs but remains substantial until 5,000 TCs, compared to that of R_s. When counting effects of increase in both R_s and I_o in the experiments, it is expected that the power decreases to in the range of 83 to 90 % at 3,000 TC, and in the range of 68 to 87 % at 5,000 TC depending on the regression models of R_s and I_o, as shown in Fig. 15.

V. ASSESSMENT OF POWER DROP FUNCTION

The mathematical form of the power drop is a crucial issue in the prediction of the solar module's power output [9]. In this section, a goodness-of-fit analysis of the power drop is conducted to assess appropriate functional models of it. The function for the power drop should be decreasing over TC

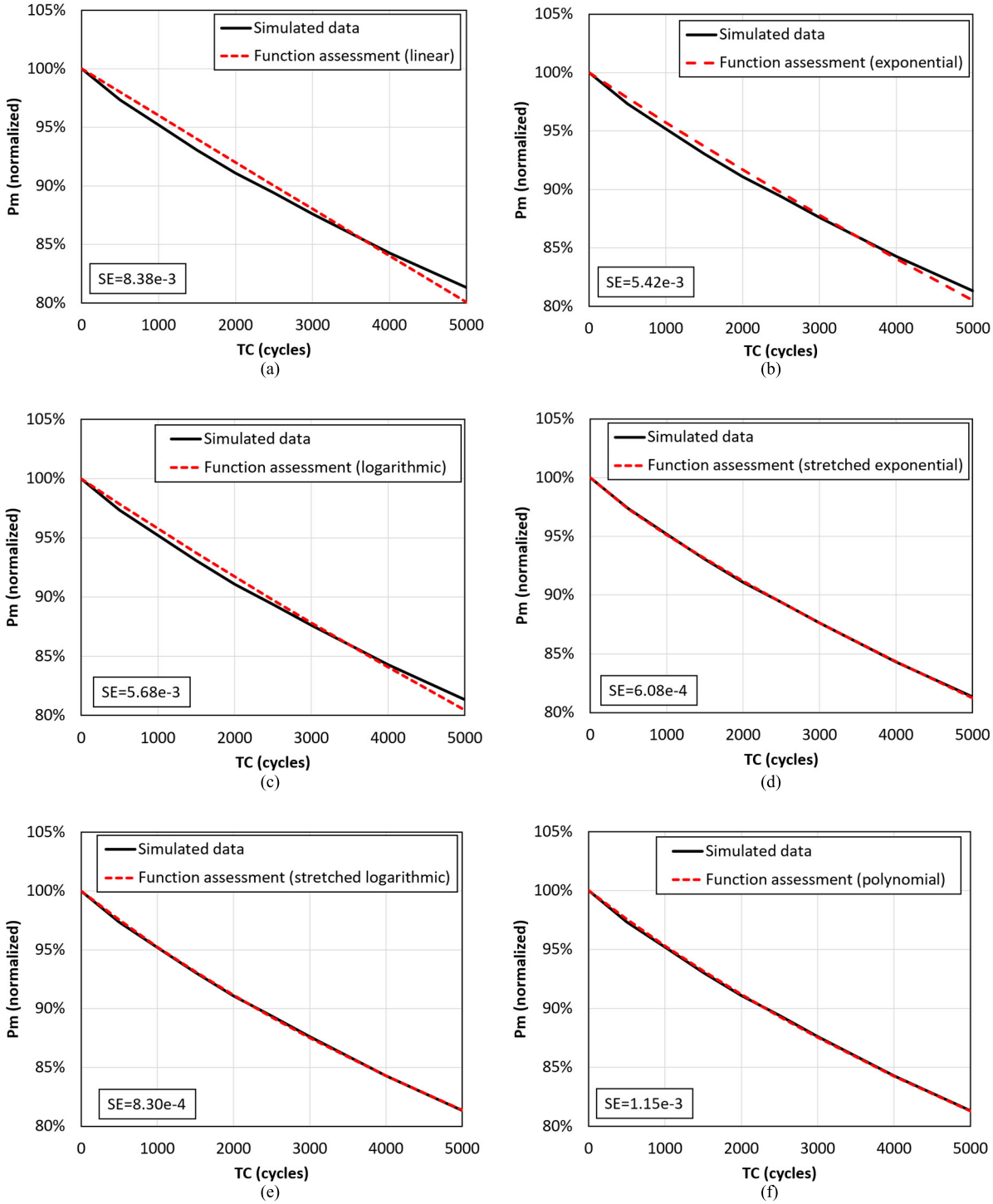

FIGURE 16. Goodness-of-fit analysis results of power drop over TC with (a) linear, (b) exponential, (c) logarithmic, (d) stretched exponential, (e) stretched logarithmic, and (f) polynomial functions when linear increasing is assumed for R_S and I_O.

and have a value of 1 at time zero. Based on these conditions, seven possible models were selected:

Model 1 (linear model):

$$\frac{P_m(N)}{P_m(0)} = CN + 1, \tag{13a}$$

Model 2 (exponential model):

$$\frac{P_m(N)}{P_m(0)} = exp(-CN), \tag{13b}$$

Model 3 (logarithmic model):

$$\frac{P_m(N)}{P_m(0)} = -ln(CN + 1) + 1, \tag{13c}$$

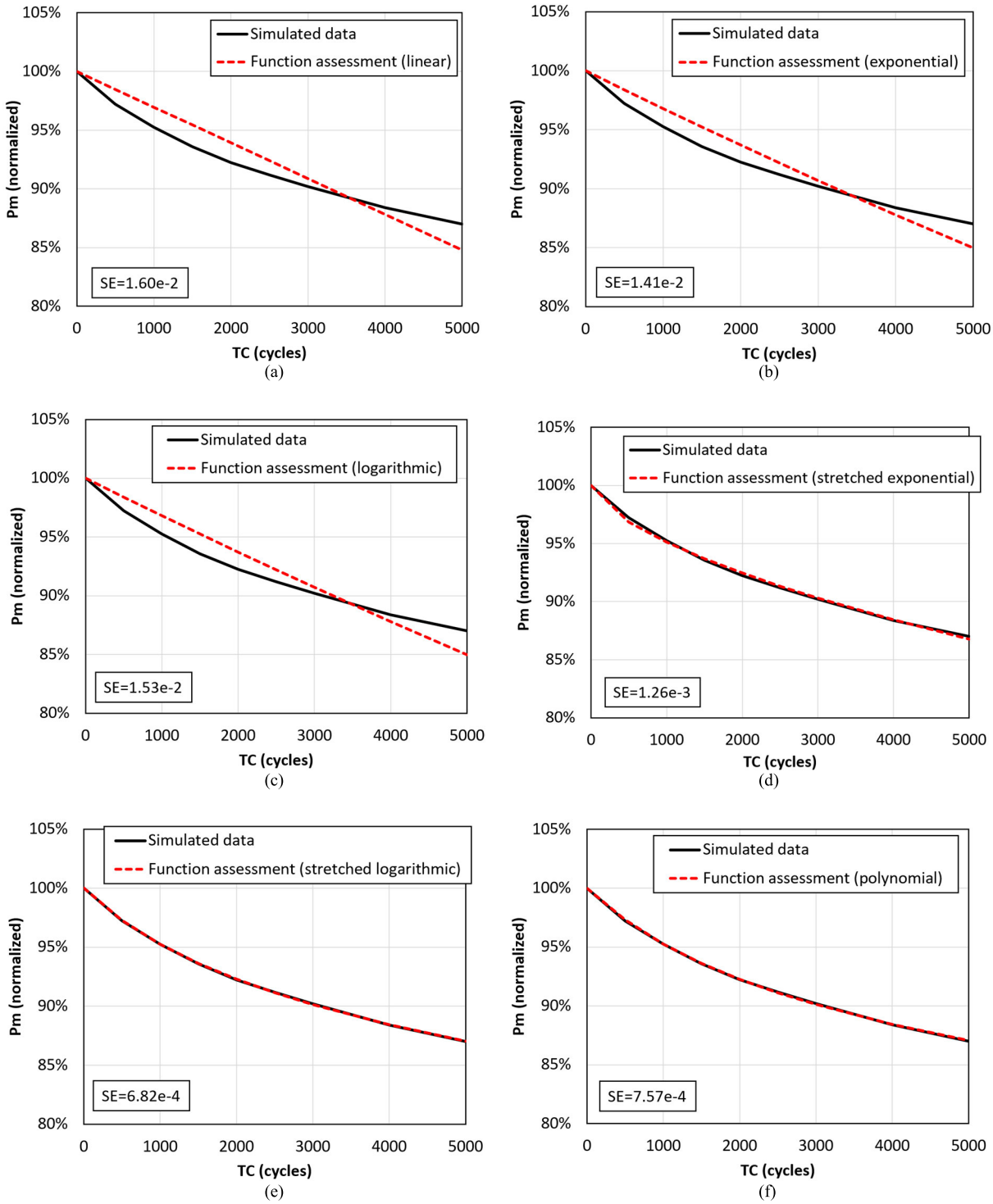

FIGURE 17. Goodness-of-fit analysis results of power drop over TC with (a) linear, (b) exponential, (c) logarithmic, (d) stretched exponential, (e) stretched logarithmic, and (f) polynomial functions when logarithmic increasing is assumed for R_S and I_o.

Model 4 (stretched exponential model):

$$\frac{P_m(N)}{P_m(0)} = exp\left(-(CN)^n\right), \tag{13d}$$

Model 5 (stretched logarithmic model):

$$\frac{P_m(N)}{P_m(0)} = -ln(CN+1)^n + 1, \tag{13e}$$

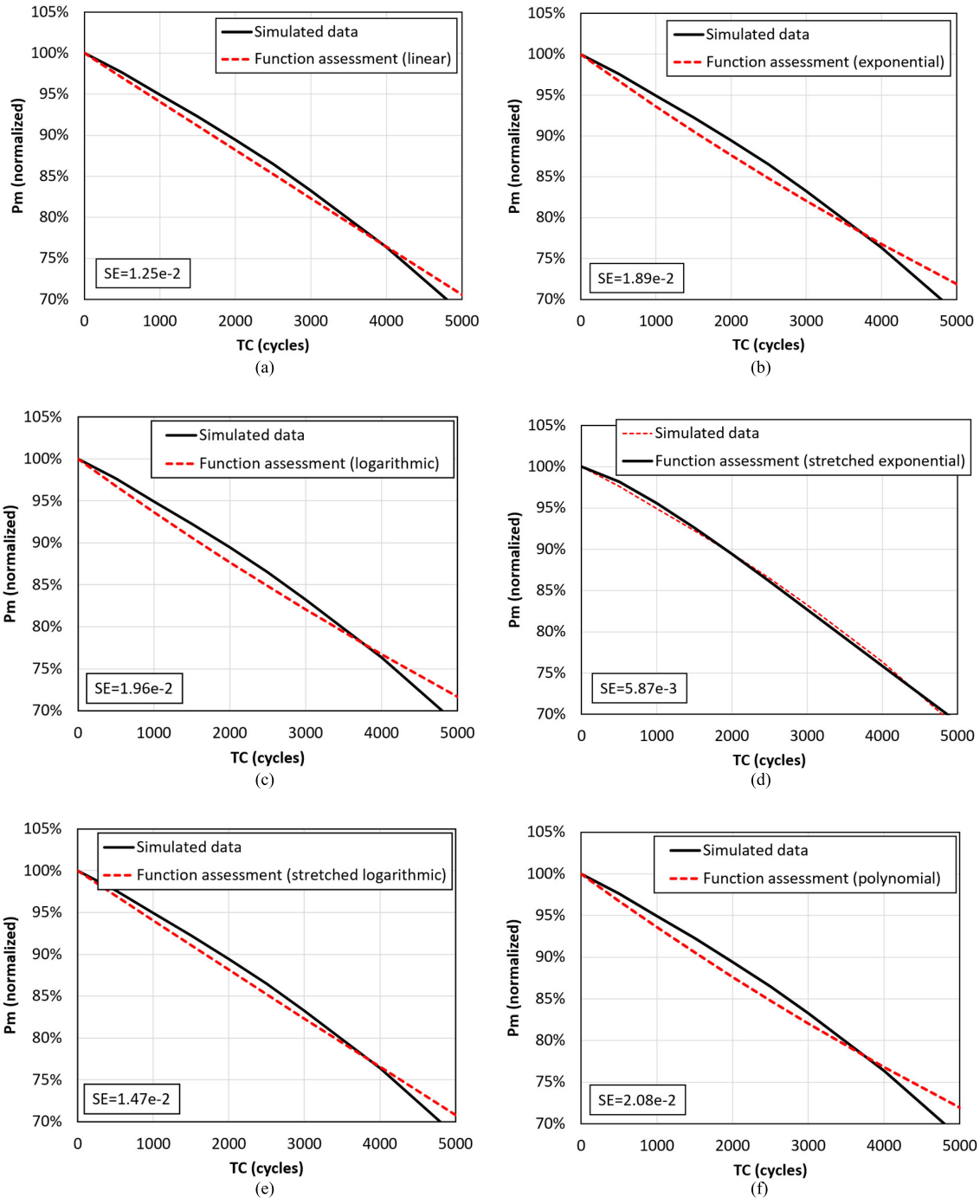

FIGURE 18. Goodness-of-fit analysis results of power drop over TC with (a) linear, (b) exponential, (c) logarithmic, (d) stretched exponential, (e) stretched logarithmic, and (f) polynomial functions when exponential increasing is assumed for R_s and I_o.

Model 6 (polynomial model):

$$\frac{P_m(N)}{P_m(0)} = \frac{1}{(CN+1)^n}, \tag{13f}$$

where N is the number of TCs, and C and n are the model constants. The nonlinear least squares method in MATLAB [20] was used to obtain the model constants with the solid line data of Fig. 15. The results are represented in Fig. 16 to 18 with the linear, logarithmic, and exponential models of R_s and I_o. Regardless of model types, the linear, exponential, and logarithmic functions exhibit large deviations. These functions can either overestimate or underestimate the power drop, depending on the model types and number of TC. Standard errors between the function assessments and simulated data were calculated and summarized at Fig. 19. Among the seven models, the stretched exponential function will be the best selection since it can fit in any case.

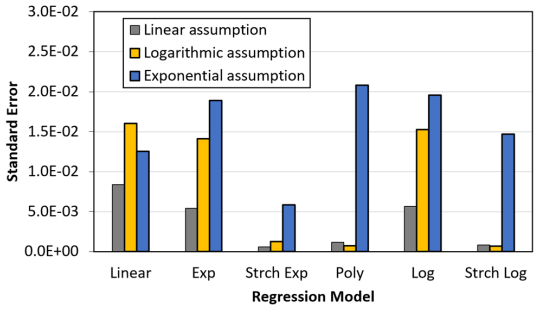

FIGURE 19. **Comparison of standard errors for the regression using seven functions.**

VI. CONCLUSION

TC experiments were conducted on two sets of Si one-cell solar modules following the IEC 61215 standard. After 1,000 TC, P_m decreased to a range of 92–96 %. The decrease in P_m was primarily attributed to the decrease in FF, but V_{oc} also decreased significantly. To accurately track the changes in R_s and I_o in the diode equivalent circuit model during TC, a novel method of extracting the parameters using all experimental data points, not just the selected ones, of the I-V curve was introduced and implemented. The observations revealed that both I_o and R_s increased during TC. Over 1,000 TCs, R_s and I_o increased between 13–42 % and 38–83 %, respectively. The increases were analyzed numerically and experimentally.

When evaluating three functions – linear, exponential, and logarithmic – for the increases in R_s and I_o, the predicted increases were calculated as ranging between 92–231 % for R_s and 153–878 % for I_o after 5,000 TC. If only R_s increases with TC and I_o remains unchanged, it is expected that the power output will decrease to between 82–93 % after 5,000 TC. Conversely, if only I_o increases with TC and R_s remains unchanged, it is expected that the power output will decrease to between 86–94 % after 5,000 TC. Based on these studies, it can be concluded that the power drop mechanism of solar cells under TC is influenced by the increases in both R_s and I_o, which are caused by the cracking of the solder layer. In addition, a goodness-of-fit analysis revealed that a stretched exponential function best represents the power drop of a solar cell under TC.

REFERENCES

[1] D. C. Jordan, T. J. Silverman, J. H. Wohlgemuth, S. R. Kurtz, and K. T. VanSant, "Photovoltaic failure and degradation modes," *Prog. Photovolt., Res. Appl.*, vol. 25, no. 4, pp. 318–326, Apr. 2017.
[2] *Terrestrial Photovoltaic (PV) Modules-Design Qualification and Type Approval—Part 1–1: Special Requirements for Testing of Crystalline Silicon Photovoltaic (PV) Modules*, Standard IEC 61215, 2021.
[3] A. Skoczek, T. Sample, E. D. Dunlop, and H. A. Ossenbrink, "Electrical performance results from physical stress testing of commercial PV modules to the IEC 61215 test sequence," *Sol. Energy Mater. Sol. Cells*, vol. 92, pp. 1593–1604, Dec. 2008.
[4] J.-S. Jeong, N. Park, and C. Han, "Field failure mechanism study of solder interconnection for crystalline silicon photovoltaic module," *Microelectron. Rel.*, vol. 52, nos. 9–10, pp. 2326–2330, Sep. 2012.
[5] J. Jeong, N. Park, W. Hong, and C. Han, "Analysis for the degradation mechanism of photovoltaic ribbon wire under thermal cycling," in *Proc. 37th IEEE Photovoltaic Specialists Conf.*, Jun. 2011, pp. 3159–3161.
[6] V. Sharma and S. S. Chandel, "Performance and degradation analysis for long term reliability of solar photovoltaic systems: A review," *Renew. Sustain. Energy Rev.*, vol. 27, pp. 753–767, Nov. 2013.
[7] S. Kumar and R. Gupta, "Thermo-mechanical degradation at finger-solder interface in a crystalline silicon photovoltaic module under thermal fatigue conditions," in *Proc. IEEE 46th Photovoltaic Specialists Conf. (PVSC)*, Jun. 2019, pp. 118–121.
[8] R. Asadpour, X. Sun, and M. A. Alam, "Electrical signatures of corrosion and solder bond failure in c-Si solar cells and modules," *IEEE J. Photovolt.*, vol. 9, no. 3, pp. 759–767, May 2019.
[9] D. C. Jordan, T. J. Silverman, B. Sekulic, and S. R. Kurtz, "PV degradation curves: Non-linearities and failure modes," *Prog. Photovolt., Res. Appl.*, vol. 25, no. 7, pp. 583–591, Jul. 2017.
[10] A. M. Humada, M. Hojabri, S. Mekhilef, and H. M. Hamada, "Solar cell parameters extraction based on single and double-diode models: A review," *Renew. Sustain. Energy Rev.*, vol. 56, pp. 494–509, Apr. 2016.
[11] C. Han, "Analysis of moisture-induced degradation of thin-film photovoltaic module," *Sol. Energy Mater. Sol. Cells*, vol. 210, Jun. 2020, Art. no. 110488.
[12] A. Kaminski, J. J. Marchand, H. El Omari, A. Laugier, Q. N. Le, and D. Sarti, "Conduction processes in silicon solar cells," in *Proc. 25th IEEE Photovoltaic Specialists Conf.*, May 1996, pp. 573–576.
[13] O. Breitenstein, J. Bauer, P. P. Altermatt, and K. Ramspeck, "Influence of defects on solar cell characteristics," *Solid State Phenomena*, vols. 156–158, pp. 1–10, Oct. 2009.
[14] C. Han, "Simulation of series resistance increase through solder layer cracking in Si solar cells under thermal cycling," *Energies*, vol. 16, no. 6, p. 2524, Mar. 2023.
[15] T. Fuyuki, H. Kondo, T. Yamazaki, Y. Takahashi, and Y. Uraoka, "Photographic surveying of minority carrier diffusion length in polycrystalline silicon solar cells by electroluminescence," *Appl. Phys. Lett.*, vol. 86, no. 26, Jun. 2005, Art. no. 262108.
[16] S. Park and C. Han, "Analysis of EL images on Si solar module under thermal cycling," *J. Mech. Sci. Technol.*, vol. 36, no. 7, pp. 3429–3436, Jul. 2022.
[17] A. Cuevas, "The recombination parameter J_0," *Energy Proc.*, vol. 55, pp. 53–62, Jan. 2014.
[18] S. Park and C. Han, "Reliability-driven design optimization of Si solar module under thermal cycling," *J. Mech. Sci. Technol.*, vol. 36, no. 8, pp. 4099–4114, Aug. 2022.
[19] *Analog Devices, LTspice*. Accessed: Nov. 2023. [Online]. Available: https://www.analog.com/en/design-center/design-tools-and-calculators/ltspice-simulator.html
[20] *MATLAB Version 9.12.0*, The MathWorks, Natick, MA, USA, 2022.

CHANGWOON HAN received the B.Sc. and M.Sc. degrees in mechanical engineering from Seoul National University, Seoul, Republic of Korea, in 1993 and 1995, respectively, and the Ph.D. degree in mechanical engineering from the University of Maryland, College Park, MD, USA, in 2005. From 2005 to 2017, he was a Principal Research Engineer with the Korea Electronics Technology Institute, Seongnam, Republic of Korea. He is currently an Associate Professor with the Department of Mechanical Engineering, The State University of New York, Korea (SUNY Korea), Incheon, Republic of Korea. His research interests include physics-of-failure, prognostics and health management, design-for-reliability, and photomechanics.

SEUNGIL PARK received the B.S. degree in electronic engineering from the Tech University of Korea, South Korea, in 2012, the M.S. degree from Hanyang University, Seoul, South Korea, in 2015, and the M.S. degree in mechanical engineering from The State University of New York, Korea (SUNY Korea), Incheon, South Korea. From 2013 to 2017, he was a Researcher with the Korea Electronics Technology Institute. Since 2023, he has been a Research Assistant with the Department of Mechanical Engineering, SUNY Korea. His research interests include accelerated lifetime test and accelerated stress test design, lifetime improvement of electronic device, module, and system, and physics-of-failure based on reliability.